

Received November 28, 2018, accepted January 4, 2019, date of publication January 18, 2019, date of current version February 6, 2019.

Digital Object Identifier 10.1109/ACCESS.2019.2893196

Terahertz Dielectric Property Characterization of Photopolymers for Additive Manufacturing

NATTAPONG DUANGRIT¹, **BINBIN HONG^{2,3}**, (Student Member, IEEE),
ANDREW D. BURNETT⁴, **PRAYOOT AKKARAEKTHALIN¹**, (Member, IEEE),
IAN D. ROBERTSON³, (Fellow, IEEE), AND
NUTAPONG SOMJIT³, (Member, IEEE)

¹Department of Electrical and Computer Engineering, King Mongkut's University of Technology North Bangkok, Bangkok 10800, Thailand

²College of Electronic Science and Technology, Shenzhen University, Shenzhen 518000, China

³School of Electronic and Electrical Engineering, University of Leeds, Leeds LS2 9JT, U.K.

⁴School of Chemistry, University of Leeds, Leeds LS2 9JT, U.K.

Corresponding author: Nattapong Duangrit (localty.j@gmail.com)

This work was supported in part by the Thailand Research Fund through the TRF Senior Research Scholar Program under Grant RTA 6080008, in part by the Royal Golden Jubilee Ph.D. Program under Grant PHD/0056/2558, and in part by the Engineering and Physical Sciences Research Council (EPSRC) under Grant EP/N010523/1, Grant EP/N005686/1, and Grant EP/P007449/1.

ABSTRACT In this paper, resin-based photocurable polymer materials for stereolithography, digital-light-processing (DLP), and polymer-jetting additive manufacturing techniques were characterized from 0.2 to 1.4 terahertz (THz) for their comprehensive dielectric properties, e.g., refractive index, absorption coefficient, dielectric constant, and loss tangent, by using laser-based THz time-domain spectroscopy. A total of 14 photocurable 3D-printing polymers were chosen, owing to their suitability, in terms of printing resolution, material characteristics, and so on, for millimeter-wave (mm-wave) and THz applications. The measurement results from 0.2 to 1.4 THz, the dielectric constants of all photopolymer samples under test are between 2.00–3.10, while the loss tangents are from 0.008 to 0.102, which are quite useful for many applications, e.g., 3D printed antennas and THz transmission lines, which were demonstrated by an asymptotically quasi-single-mode Bragg fiber microfabricated by DLP micromanufacturing technique using HTM140-V2 photopolymer, which is previously reported at the nominal frequencies from 0.246 to 0.276 THz.

INDEX TERMS Additive manufacturing, digital light processing, stereolithography, polymer jetting.

I. INTRODUCTION

Additive manufacturing technology has attracted much attention to modern three-dimensional (3D) fabrication processes due to its rapid prototyping capability, especially with a broad diversity of dielectric and metallic materials that can be used to fabricate design prototypes of almost any 3D structures. It has become even more interesting recently since it has a capability to accurately manufacture functional devices with microscale features with a good repeatability [1]–[4], which is very suitable to microfabricate functional mm-wave and THz components such as dielectric lens antennas [6]–[8], waveguides [9]–[11], sensors [9], and filters/splitters [12]–[16] for realizing low-cost complex THz systems. 3D printing techniques, normally used in mm-wave and THz technologies, are generally classified into five categories: (1) fused deposition modeling (FDM), (2) selective laser sintering (SLS), (3) stereolithographic apparatus (SLA), (4) digital-light-processing (DLP) and (5) polymer jetting (PJ).

The FDM technique achieves the lowest printing resolution along with high surface roughness, as compared to the other additive manufacturing processes. This limits their usability to bands below 400 GHz [14] owing to the large printable structure size compared to the guided wavelength and excessive propagation losses at higher frequencies caused by surface roughness. Thermoplastic materials, which generally come in filament forms, are used to manufacture 3D structures by selectively and constructively depositing the melted filament materials along pre-determined paths. General layer heights of a single FDM printed path range practically from 50 to 500 μm with the smallest achievable single layer width of approximately 100 μm^2 , which is typically limited by the nozzle size and viscosity of the melted filament materials flowing through the nozzle aperture, and the best achievable surface roughness of approximately 35 μm [17].

The SLS printing technique relies on using a high intensity laser beam, which patterns a sinter polymeric powder material layer-by-layer. This additive manufacturing

technique can achieve superior printing resolutions ranging from 20 to 80 μm , depending on the microparticle sizes of the powder material used in the fabrication processes. The SLS technique however suffers from material shrinkage of approximately 3-5% but can achieve low surface roughness of approximately 6 μm [17]. Nevertheless, there are very limited material choices of microparticle powders commercially available for the SLS technique [19], [20], restricting the usability of this additive manufacturing technology for mm-wave and THz applications.

The SLA and DLP techniques use either a laser beam or an ultraviolet (UV) light source, respectively, to micropattern a 3D structure by selectively curing resin-based photopolymer with printing resolutions dependent on the spot size used to pattern the 3D structure. Generally, a superior surface roughness of less than 10 μm can be achieved by these technologies. Moreover, the SLA technique can achieve a printing resolution of approximately 40-250 μm of the structure width and 25 μm of the structure height [21]. The best printing resolution for the DLP technique (ASIGA: PICO2 HD) are 27 μm for the structure width and 1 μm for the structure height, making them one of the most accurate and suitable additive manufacturing techniques for mm-wave and THz applications covering most signal frequencies in the THz bands ranging from 100 GHz to 1.0 THz. However, even though there is a broad choice of commercially available photopolymers, technical information regarding electromagnetic and optical material characteristics of these photocurable materials is very limited and fragmented with only a few frequency points or narrow frequency band information available for a small range of photopolymers [8], [9], and [11].

The PJ technique offers superior printing accuracy and resolutions relying on a printing principle similar to the inkjet printing process by using printhead nozzles to droplet liquid photopolymer onto a build plate and, simultaneously, the polymer materials are photocured and 3D patterned by UV light. This 3D printing technique can achieve resolutions of approximately 14 μm structure height and 23 μm structure width, respectively. Moreover, a surface roughness of smaller than 10 μm is achievable by PJ [22], [23]. Therefore, PJ is one of the most preferable additive manufacturing techniques for mm-wave and THz. However, lack of material properties available for PJ suitable materials at THz frequencies limits their usability in mm-wave and THz applications with limited and non-comprehensive electromagnetic and optical material properties currently publicly available.

This work presents uses THz time-domain spectroscopy (THz-TDS) to obtain comprehensive electromagnetic and optical material characterization of resin-based photopolymers used in SLA, DLP and PJ additive manufacturing processes between 0.2 to 1.4 THz. Fourteen photopolymer specimens were characterized for their refractive index, absorption coefficient, dielectric constant and loss tangent. To demonstrate the usability of the photopolymers in this work, an asymptotically single-mode all-photopolymer Bragg fiber fabricated by using HTM140-V2 photocurable

polymer, which was previously reported [11], is also briefly discussed in this paper in the context of this new data.

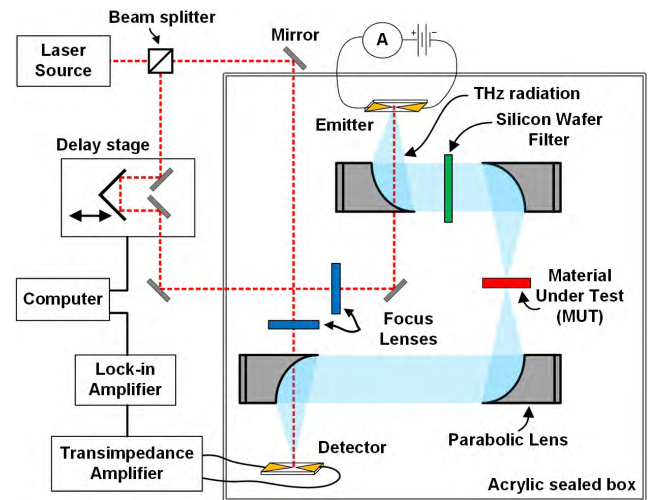


FIGURE 1. Working principle of the THz-TDS measurement system used in this work which is similar to those use in [24]–[26].

II. METHODOLOGY

A. THz TIME-DOMAIN SPECTROSCOPY SYSTEM

A schematic diagram showing the working principle of the free-space THz-TDS system, used in this work, is shown in Fig. 1 [24]–[26]. The laser source is a commercial, mode-locked Ti:Sapphire (Coherent Vitar-T-HP), operating at 800 nm, with a repetition rate of 80 MHz, pulse width of 20 fs and an average power between $\sim 1\text{W}$ [27]. Both the THz emitter and detector in this system are photoconductive antennas (PCA) made of low-temperature-grown GaAs (LT-GaAs) transferred onto 5 mm z-cut quartz substrates. Each switch consists of two bow-tie shaped Ti:Au electrodes with a 200 μm gap between them [24].

The initial laser beam is divided into two beams using an 80:20 beam splitter, with the higher power beam used to generate the THz pulse and the weaker beam used for gated detection. The pump beam is focused, using a lens, onto a PCA biased at 350 V electrically chopped at 10 KHz, which is used to generate the THz radiation. The THz radiation is then collected, collimated and focussed by a set of off-axis parabolic mirrors. A silicon wafer is used to block any stray laser light reflected from the emitter surface from reaching the PCA detector while transmitting the majority of the THz radiation. The THz radiation is focused onto the sample, after which a second set of off-axis parabolic mirrors are used to re-collimate and then focus the THz transmitted through the sample onto the second PCA for detection. The probe beam is also focused onto the PCA detector using a lens, and when both the probe pulse and THz radiation are incident on the detector, the THz field at that point in time can be measured, as the fs probe pulse is much shorter in time than the THz pulse. By delaying the pump beam with a linear delay stage, the point in time where the THz and probe beams are both incident changes, allowing for a time domain signal

of the THz beam to be obtained. The output signal from the PCA detector is first amplified using a transimpedance amplifier and measured using a lock-in amplifier referenced to the 10 KHz bias of the THz PCA emitter. The THz optical section is placed within an acrylic box which is purged with dry air. This reduces the atmospheric water vapor in the system, which strongly absorbs THz radiation, thus increasing transmitted THz field at the detector.

B. METHODOLOGY FOR MATERIAL CHARACTERIZATION

THz-TDS is a coherent material characterization technique, which allows both the amplitude and phase of the THz signal propagating through the material-under-test (MUT) to be simultaneously measured which in turn allows both the complex dielectric constant and loss tangent to be extracted numerically. The mathematical relationship between the complex dielectric constant, $\tilde{\epsilon}(\omega)$, and the fundamental optical characteristic, $\tilde{n}(\omega)$, is described as $\tilde{\epsilon}(\omega) = (\tilde{n}(\omega))^2$, where ω is the angular frequency [28], [29].

At the photodetector in Figure 1, the complex frequency spectra of the reference THz signal without the MUT specimen $\tilde{S}_r(\omega)$ and with the MUT specimen $\tilde{S}_s(\omega)$ can be analytically calculated by transforming the measured receive signals from the time domain to the frequency domain by using a Fourier transform. The ratio of $\tilde{S}_s(\omega)$ and $\tilde{S}_r(\omega)$ are represented by the magnitude, $\rho(\omega)$, and phase, $\phi(\omega)$ [30], as follows:

$$\frac{\tilde{S}_s(\omega)}{\tilde{S}_r(\omega)} = \rho(\omega) \cdot e^{-j\phi(\omega)} \tag{1}$$

From the relationship from (1), the refractive index ($n_s(\omega)$) and extinction coefficient ($k_s(\omega)$) can be calculated by using the following equations:

$$n_s(\omega) = \phi(\omega) \cdot \frac{c_0}{d} + 1 \tag{2}$$

and

$$k_s(\omega) = \ln \left(\frac{4 \cdot n_s(\omega)}{\rho(\omega) \cdot (n_s(\omega) + 1)^2} \right) \cdot \frac{c_0}{\omega d} \tag{3}$$

where d is thickness of the specimen (cm), c_0 is the velocity of light in vacuum. The extinction coefficient (k_s) can be expressed in term of the absorption coefficient, α (cm^{-1}), by:

$$k_s(\omega) = \frac{\alpha(\omega) \cdot c_0}{2\omega} \tag{4}$$

and

$$\alpha(\omega) = \frac{2}{d} \cdot \ln \left(\frac{4n_s(\omega)}{\rho(\omega) \cdot (n_s(\omega) + 1)^2} \right) \tag{5}$$

The complex dielectric constant can be normally represented by $\tilde{\epsilon}(\omega) = \epsilon'(\omega) - j \cdot \epsilon''(\omega)$, where ϵ' and ϵ'' are the real and imaginary parts, respectively, and thus the loss tangent ($\tan \delta$) is calculated by ϵ''/ϵ' . Therefore, the real part, $\epsilon'(\omega)$, and imaginary part, $\epsilon''(\omega)$, of the complex dielectric constant are calculated by:

$$\epsilon'(\omega) = (n_s(\omega))^2 - (k_s(\omega))^2 = (n_s(\omega))^2 - \left(\frac{c_0 \cdot \alpha(\omega)}{2\omega} \right)^2 \tag{6}$$

and

$$\epsilon''(\omega) = 2 \cdot n_s(\omega) \cdot k_s(\omega) = \frac{c_0 \cdot n_s(\omega) \cdot \alpha_s(\omega)}{\omega} \tag{7}$$

TABLE 1. List of selected photopolymers used in this work.

Specimen	Printing technique	Manufacturer	Thickness (mm)
Gray resin	SLA	Formlabs	2.98
RGD430	PJ	Stratasys	0.99
RGD450	PJ	Stratasys	0.98
RGD835	PJ	Stratasys	0.99
ABS Flex	PJ	Stratasys	1.05
LS600	PJ	Stratasys	1.06
ABS Tough	DLP	EnvisionTEC	2.84
ABS Flex Black	DLP	EnvisionTEC	2.97
Photosilver	DLP	EnvisionTEC	2.82
HTM140V2	DLP	EnvisionTEC	2.80
RC-31	DLP	EnvisionTEC	2.96
RC-70	DLP	EnvisionTEC	2.92
RC-90	DLP	EnvisionTEC	2.83
R11	DLP	EnvisionTEC	2.84

III. RESULTS

A. PHOTOPOLYMER SPECIMEN SELECTION

Table 1 shows the names and manufacturers of all fourteen selected photopolymer specimens with specimen thicknesses used during the THz-TDS measurement. The specimen thicknesses first determined accurately using a digital micron-scale Vernier caliper prior to each measurement and then confirmed using a total variance analysis method similar to that described in [31]. Gray resin fabricated using SLA technique is provided by Formlabs [32] while RGD-series and LS600 based on PJ printing are provided by Stratasys [33]. EnvisionTech [34] also offers a broad range of different photocurable resin polymers e.g. ABS series, Photosilver, HTM140-V2, RC-series, and R11. All photopolymer specimens were provided as a large square ($\sim 7.5\text{cm}^2$). To make mounting in the THz-TDS straightforward a ~ 1 -inch disk was cut out of each sample using a pillar drill with the spin speed of 4,500 rev/min and then cleaned by dipping into isopropyl alcohol and then immediately rinsing in deionized water before being dried in a clean environment at room temperature using laboratory-grade dry compressed air. The THz-TDS measurement setup used to characterize these photopolymer specimens is shown in Fig. 1.

B. REFRACTIVE INDICES

Figure. 2 shows the refractive indices of all fourteen photocurable polymer specimens from 0.2-1.4 THz. At 1.4 THz the values of refractive indices of all photopolymer specimens decrease slightly, as compared to their nominal values

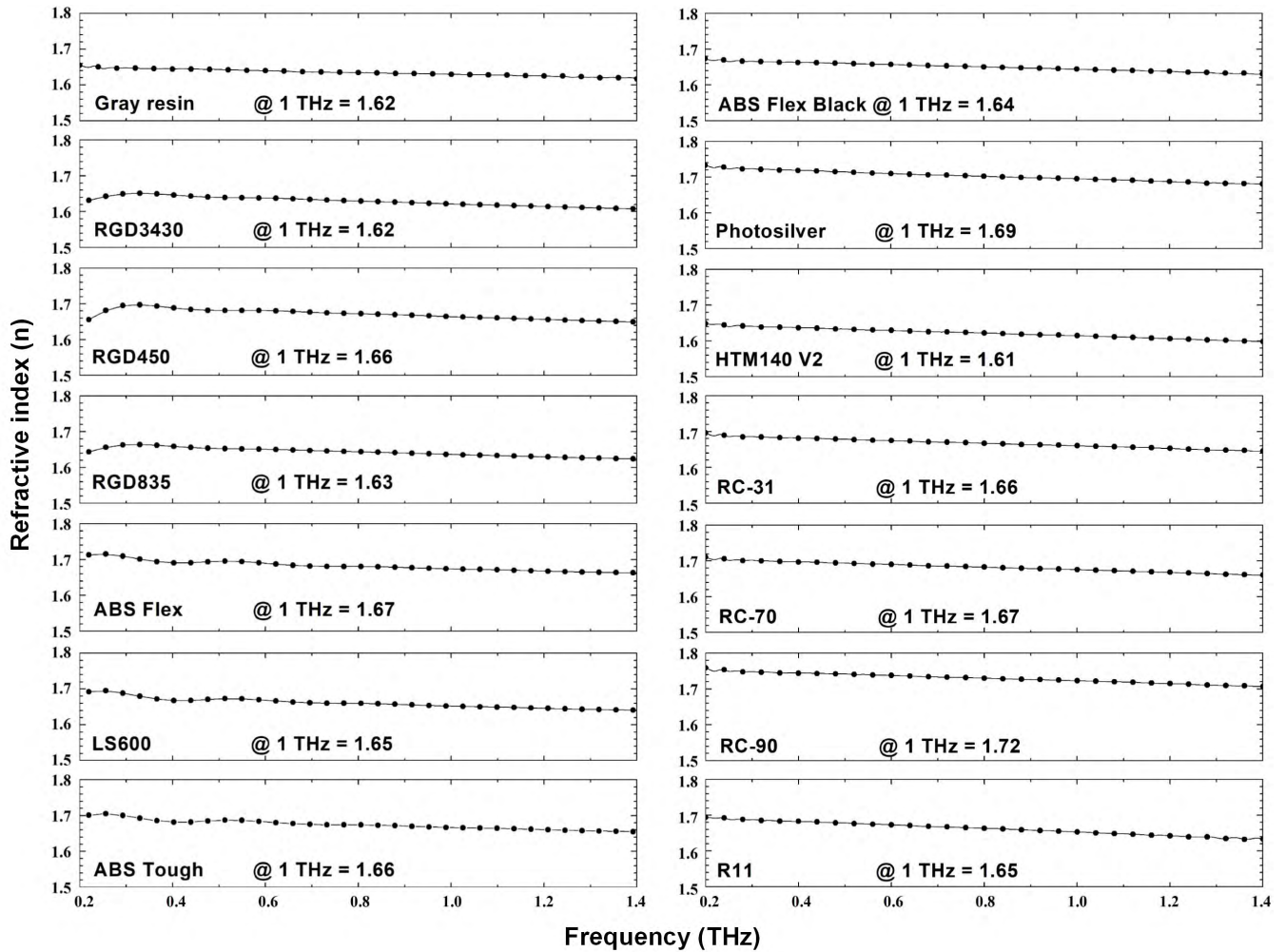


FIGURE 2. Measured refractive indices of fourteen selected photocurable polymer specimens from 0.2-1.4 THz.

at 0.2 THz, with an average change of approximately below 2%. For example, at 0.2 THz, the refractive index of the Gray resin photopolymer is 1.66, while the value decreases to 1.62 at 1.4 THz. Most of the photopolymer, including Gray resin, RGD series, LS600, ABS Tough, ABS Flex Black, HTM140-V2, RC-31, RC-70 and R11, have a refractive indices between 1.6-1.72 over the whole frequency band. The refractive indices of Photosilver and RC-90, however, range between 1.7-1.8 for the whole frequency band.

C. ABSORPTION COEFFICIENTS

The absorption coefficients from 0.2-1.4 THz of all fourteen selected photopolymers are presented in Fig 3a-3c. From Fig. 3a, the measurement results of the absorption coefficients of Gray resin, RGD series and flexible photopolymer ABS Flex were characterized. At 1.4 THz, RGD450 has the highest absorption coefficient of 39.6 cm⁻¹, followed by ABS Flex, RDG430, RGD835 and Gray resin with absorption coefficients of 36.8 cm⁻¹, 34.2 cm⁻¹, 32.7 cm⁻¹ and 33.0 cm⁻¹, respectively. Fig. 3b also plots the absorption coefficients versus frequencies for LS600, ABS Tough, ABS Flex Black,

Photosilver and HTM140-V2. At 1.4 THz, LS600 has the lowest absorption coefficient of 30.2 cm⁻¹ while those for HTM140-V2 and ABS Tough are 33.3 cm⁻¹ and 34.9 cm⁻¹, respectively. ABS Flex Black and Photosilver appear to have the absorption coefficient of 37.5 cm⁻¹ and 36.1 cm⁻¹ at 1.4 THz. In Fig. 3c, absorption coefficients of RC series and R11 are plotted. At 1.4 THz, R11 clearly has the highest absorption coefficient of 48.8 cm⁻¹ as compared to the coefficients of 37.5 cm⁻¹ for RC-90 and 34.8 cm⁻¹ for both RC-31 and RC-70. Noticeably, RC-31 and RC-90 appear to have the same figure of the absorption coefficient over the whole THz band from 0.2- 1.4 THz. In general, for the whole measurement frequencies, LS600 has the lowest absorption coefficient as compared to the rest of the photopolymer specimens while R11 appears to have the largest THz absorption coefficient.

D. DIELECTRIC CONSTANTS

From the measured refractive indices and absorption coefficients, equation (6), described in the Method section, is used to calculate the dielectric constants of the fourteen

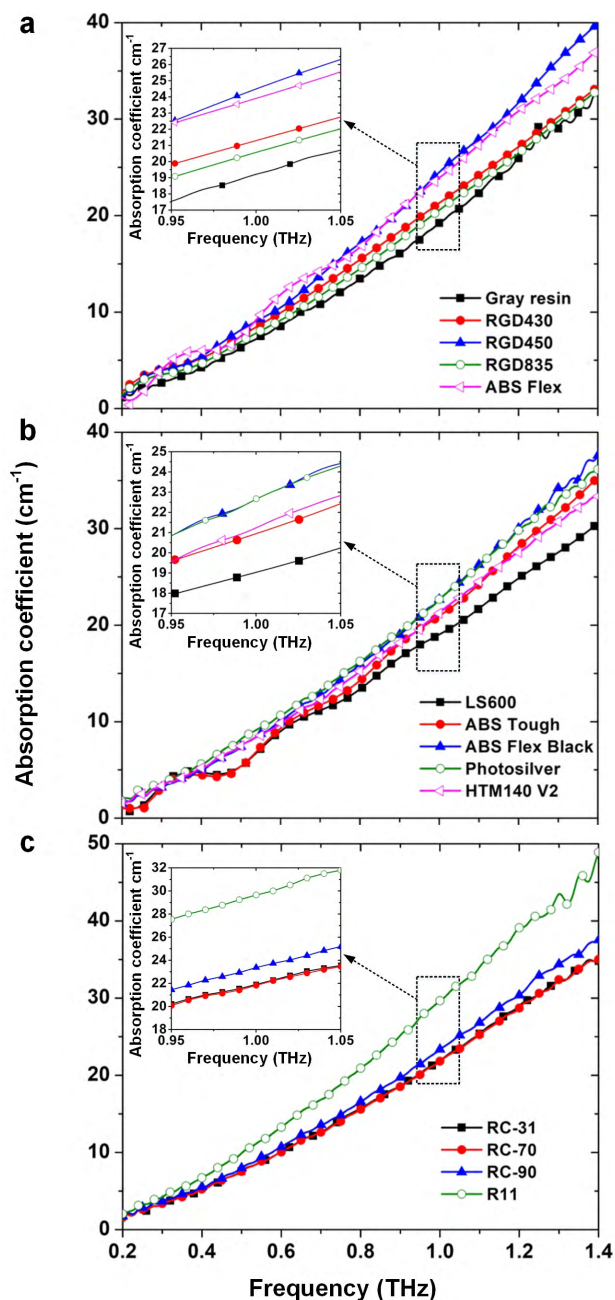


FIGURE 3. Measured absorption coefficients of 14 photopolymers.

selected photopolymers, which are shown in Fig. 4a–4c. Fig. 4a shows the dielectric constants of Gray resin, RGD series and ABS Flex. At 0.2 THz, RGD430 has the lowest dielectric constant of 2.70 while highest value belongs to ABS Flex at 2.94. At 1.4 THz, all the dielectric constants for Gray resin, RGD430, RGD450, RGD835 and ABS Flex slightly decrease to 2.61, 2.58, 2.71, 2.63 and 2.76 as compare to their nominal figures at 0.2 THz, respectively. In Fig. 4b, dielectric constants of LS600, ABS Tough, ABS Flex Black, Photosilver and HTM140-V2 are shown. At 0.2 THz, the dielectric constants of LS600, ABS Tough, ABS Flex Black, Photosilver and HTM140-V2 are 2.86, 2.89, 2.80, 3.00, 2.71, respectively, while these figures slightly decrease

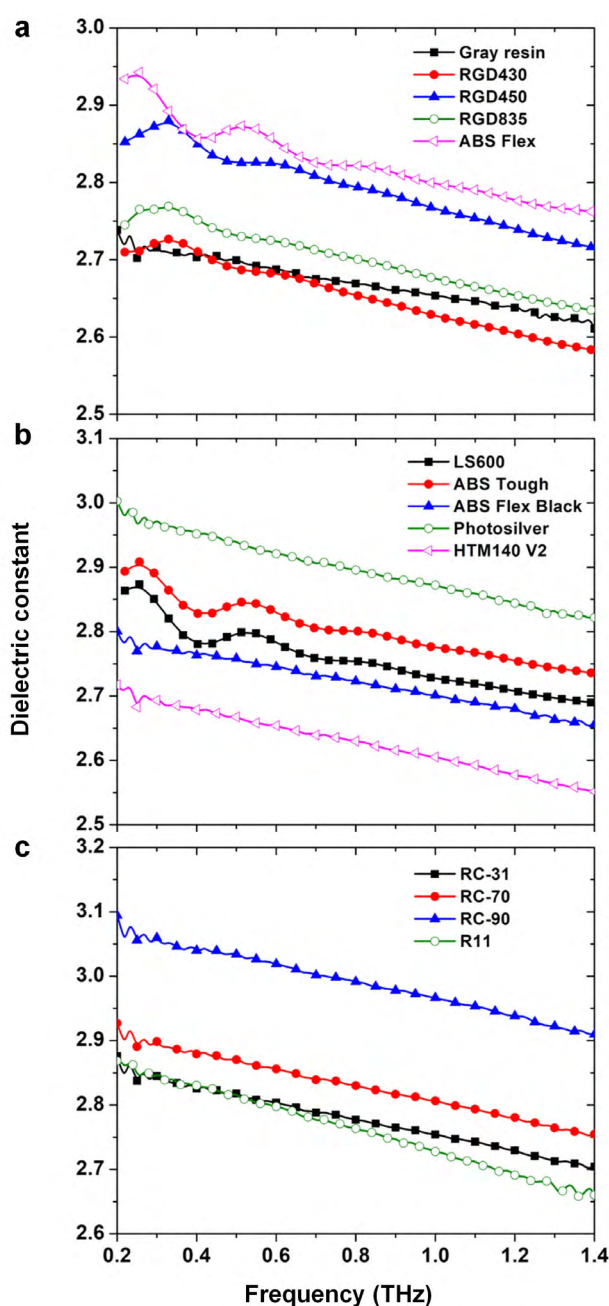


FIGURE 4. Measured dielectric constants of the photocurable polymers.

to 2.68, 2.73, 2.65, 2.82, 2.55, at 1.4 THz. Fig. 4c shows the dielectric constant plots of RC series and R11 photopolymers. R11 and RC-31 photopolymers have the same dielectric constants of 2.87 at the frequency of 0.2 THz and slightly decrease to 2.66 and 2.70, respectively, at 1.4 THz. Moreover, dielectric constants of 2.92 and 3.09 at 0.2 THz and 2.75 and 2.90 at 1.4 THz for RC-70 and RC-90, respectively. From the calculated figures of the dielectric constants plotted in Fig. 4a-4c, the photocurable polymers measured here have a very strong potential to be used for developing a number of THz and mm-wave passive components and functional devices ranging from THz transmission lines to THz antennas.

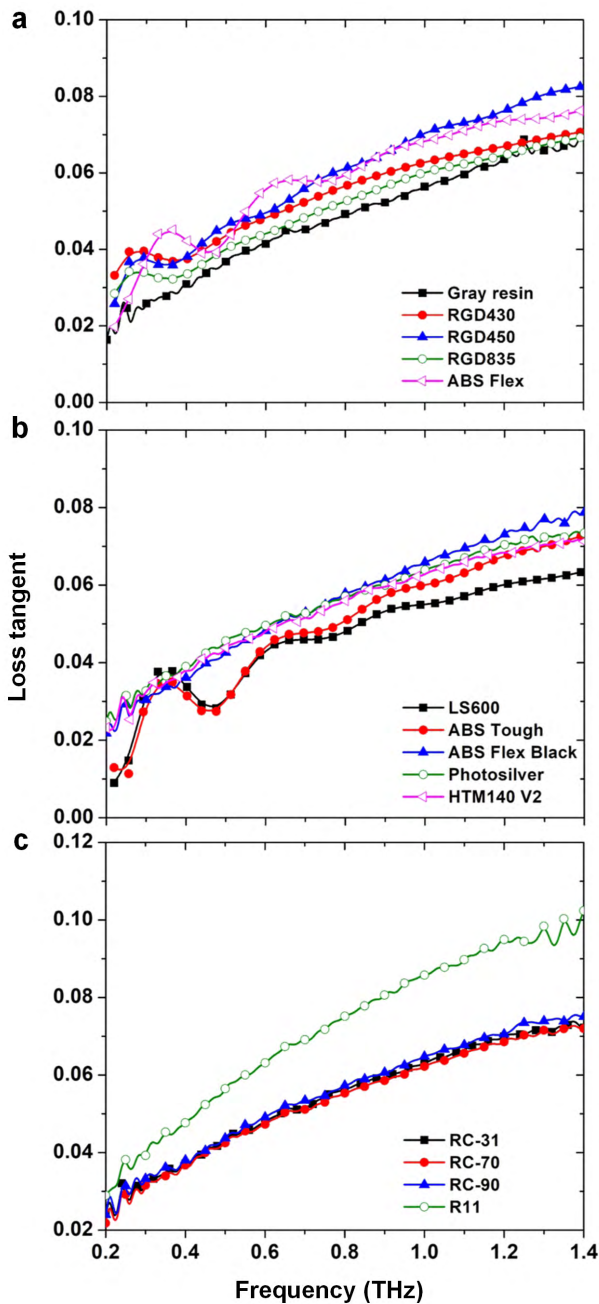


FIGURE 5. Measured loss tangents of the selected photopolymers.

E. LOSS TANGENTS

Fig. 5a-5c shows the loss tangents, which are used to determine the material loss characteristics, of all selected photopolymers. From Fig. 5a, Gray resin, RGD430, RGD450, RGD835 and ABS Flex have loss tangents of 0.016, 0.033, 0.025, 0.028 and 0.019, at 0.2 THz, respectively, and these values increase to 0.069, 0.071, 0.082, 0.069 and 0.076 at 1.4 THz. Loss tangents of LS600, ABS Tough, ABS Flex Black, Photosilver and HTM140-V2 are plotted in Fig. 5b. At 0.2 THz, the loss tangents of ABS Flex Black, Photosilver and HTM140-V2 are very close to each other at approximately 0.023, while LS600 and ABS Tough have lower loss

tangent of 0.008 and 0.012. At 1.4 THz, ABS Flex Black has the highest loss tangent of 0.078 and LS600 has the lowest one of 0.063. ABS Tough, Photosilver and HTM140-V2 have very close loss tangent values of approximately 0.072 at 1.4 THz. Fig. 5c plots the loss tangent curves for RC series and R11 photopolymers. For the whole frequency band from 0.2-1.4 THz, the RC series polymers have almost the same figure for their loss tangents of approximately 0.022 and 0.073, respectively. As shown in Fig. 5c, R11 photopolymer has the highest average loss tangent as compared to the other thirteen selected photopolymers ranging from 0.028 at 0.2 THz to 0.102 at 1.4 THz, making this photocurable polymer least suitable for mm-wave and THz applications as compared to the other selected photopolymer specimens.

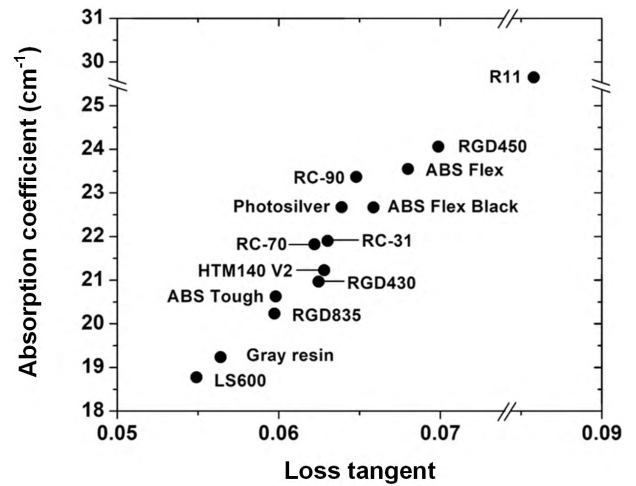


FIGURE 6. Relationship between absorption coefficients and loss tangents of the selected photopolymers at 1 THz.

Fig. 6 shows a plot of absorption coefficient versus loss tangent for all fourteen selected photopolymer specimens at 1 THz. From the measurement setup, the THz-TDS system was primarily used to measure both refractive index and absorption coefficient. Both measured material properties can be used to calculate the dielectric constant and loss tangent of the materials by using equations (6) and (7). Therefore, Fig. 6 shows a strong linear relationship between the absorption coefficient and loss tangent by showing that the material that has high absorption coefficient also has high loss tangent and vice versa.

Furthermore, a comprehensive optical and electromagnetic characteristic of these photopolymers are tabulated in Table 2 at 0.2, 0.8 and 1.4 THz. From the loss tangent and dielectric constant characteristics, all selected photocurable polymer specimens are suitable to be used in mm-wave and THz applications, which was demonstrated in the next section.

F. APPLICATIONS OF PHOTOPOLYMERS: TERAHERTZ BRAGG FIBERS

To demonstrate the usability of the selected photopolymers, HTM140-V2 was used to fabricate an asymptotically

TABLE 2. Summarized electromagnetic and optical dielectric properties of selected photopolymers.

Specimens name	Refractive index			Absorption coefficient (cm ⁻¹)			Dielectric constant			Loss tangent		
	Frequency (THz)			Frequency (THz)			Frequency (THz)			Frequency (THz)		
	0.2	0.8	1.4	0.2	0.8	1.4	0.2	0.8	1.4	0.2	0.8	1.4
Gray resin	1.654	1.634	1.616	1.133	13.470	33.005	2.738	2.669	2.610	0.016	0.049	0.069
RGD430	1.631	1.629	1.608	3.474	15.592	34.204	2.709	2.653	2.583	0.033	0.056	0.071
RGD450	1.655	1.672	1.649	3.314	17.294	39.609	2.852	2.793	2.716	0.025	0.061	0.082
RGD835	1.643	1.643	1.624	3.037	14.623	32.756	2.745	2.700	2.634	0.028	0.052	0.069
ABS Flex	1.712	1.680	1.663	1.817	16.867	36.898	2.934	2.821	2.762	0.019	0.059	0.076
LS600	1.692	1.659	1.640	1.345	13.499	30.266	2.863	2.753	2.689	0.008	0.048	0.063
ABS Tough	1.701	1.674	1.655	1.036	14.416	34.982	2.893	2.800	2.735	0.012	0.051	0.072
ABS Flex Black	1.673	1.650	1.630	1.528	16.010	37.589	2.807	2.722	2.656	0.021	0.057	0.078
Photosilver	1.732	1.702	1.680	1.802	16.260	36.148	3.002	2.895	2.821	0.024	0.057	0.073
HTM140 V2	1.648	1.622	1.598	1.602	15.219	33.345	2.717	2.630	2.551	0.023	0.056	0.071
RC-31	1.695	1.667	1.645	1.714	15.722	34.810	2.875	2.777	2.704	0.024	0.056	0.072
RC-70	1.710	1.682	1.660	1.561	15.585	34.87	2.926	2.829	2.754	0.021	0.055	0.072
RC-90	1.759	1.730	1.707	1.768	16.603	37.527	3.094	2.991	2.909	0.023	0.057	0.075
R11	1.693	1.663	1.633	2.052	20.915	48.894	2.868	2.763	2.660	0.028	0.075	0.102

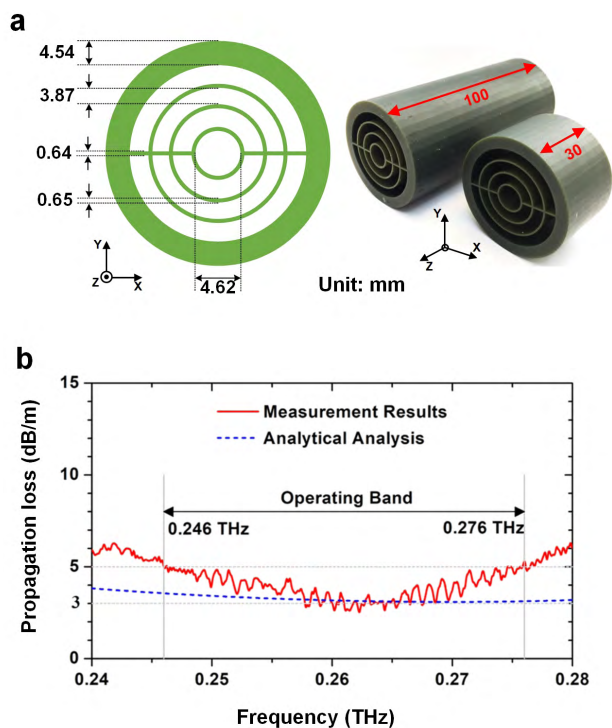


FIGURE 7. Asymptotically single-mode Bragg fiber additive-manufactured by using HTM140-V2 photopolymer. (a) cross-sectional dimensions of the all-dielectric Bragg fiber (left) and its fabricated prototype (right). (b) propagation loss characteristic of the Bragg fiber.

single-mode all-dielectric Bragg fiber with an operational frequency band from 0.246-0.276 THz, which was previously reported [11]. Fig. 7a shows the cross-sectional geometries

and dimensions of the THz Bragg fiber and the fabricated prototype with two different fiber lengths of 30 and 100 mm. EnvisionTEC HTM140-V2 photopolymer was chosen due to its high refractive index to provide cladding layers, the outermost protective layer, and the support bridges, while air gaps provided the low refractive index cladding layers. Compared to other well-known low-loss THz polymers [35], such as TOPAS, Zeonex, HDPE, and PTFE, the material attenuation of HTM140-V2 is much higher, which is a common limitation of most commercially available photopolymers in 3D printing applications to date. However, since the EM field in the Bragg fibre is tightly confined and mainly propagates inside the low-loss air core, only a small portion of the EM field is distributed in the periodic cladding material, and thereby the deleterious impact of the relatively high material attenuation of HTM140-V2 is mitigated by the air-core Bragg fibre design. The Bragg fiber prototype was fabricated by using EnvisionTEC Perfactory 3 mini multi-lens 3D printer based on DLP additive manufacturing technique. Then, the THz fiber prototype was characterized for its figure-of-merits by using free-space measurement platform together with Keysight PNA-X and OML frequency extenders operating from 0.22 to 0.325 THz. Fig. 7b shows the propagation loss characteristics of the THz electromagnetic wave along the THz Bragg fiber from 0.24- 0.28 THz. The measurement results show that the average electromagnetic propagation loss of the asymptotically single-mode Bragg fiber is lower than 5 dB/m for the nominal frequencies from 0.246 to 0.276 THz, which is the lowest propagation loss reported to date for asymptotically single-mode all-dielectric fiber at this frequency band.

IV. CONCLUSIONS

Fourteen photocurable polymer specimens for SLA, DLP and PJ additive manufacturing were characterized for their optical and electromagnetic properties from 0.2 – 1.4 THz by using laser-based THz-TDS technique. The measurement results show that all selected photopolymer specimens in this works are suitable for developing various passive mm-wave and THz components with excellent figure-of-merit as demonstrated in the previously published work on low-loss 0.2-THz asymptotically single-mode Bragg fiber fabricated by using HTM140-V2 photopolymer.

ACKNOWLEDGMENT

The data associated with this paper are openly available from the University of Leeds repository. <https://doi.org/10.5518/440>

REFERENCES

- [1] L. Min, "Novel materials, fabrication techniques and algorithms for microwave and THz components, systems and applications," Ph.D. dissertation, Dept. Elect. Comput. Eng., Univ. Arizona, Tucson, AZ, USA, 2016.
- [2] W. J. Otter and S. Lucyszyn, "Hybrid 3-D-printing technology for tunable THz applications," *Proc. IEEE*, vol. 105, no. 4, pp. 756–767, Apr. 2017.
- [3] B. Zhang, W. Chen, Y. Wu, K. Ding, and R. Li, "Review of 3D printed millimeter-wave and terahertz passive devices," *Int. J. Antennas Propag.*, vol. 2017, Jul. 2017, Art. no. 1297931.
- [4] H. Xin and M. Liang, "3-D-printed microwave and THz devices using polymer jetting techniques," *Proc. IEEE*, vol. 105, no. 4, pp. 737–755, Apr. 2017.
- [5] C. A. Fernandes, E. B. Lima, and J. R. Costa, "Dielectric lens antennas," in *Handbook of Antenna Technologies*. Lisbon, Portugal: Univ. Lisbon, 2014, pp. 1–54.
- [6] A. Vorobyov, J. R. Farserotu, and J.-D. Decotignie, "3D printed antennas for Mm-wave sensing applications," in *Proc. 11th Int. Symp. Med. Inf. Commun. Technol. (ISMICT)*, Feb. 2017, pp. 23–26.
- [7] H. Yi, S.-W. Qu, K.-B. Ng, C. H. Chan, and X. Bai, "3-D printed millimeter-wave and terahertz lenses with fixed and frequency scanned beam," *IEEE Trans. Antennas Propag.*, vol. 64, no. 2, pp. 442–449, Feb. 2016.
- [8] W. D. Furlan et al., "3D printed diffractive terahertz lenses," *Opt. Lett.*, vol. 41, no. 8, pp. 1748–1751, Apr. 2016.
- [9] J. Li, K. Nallappan, H. Guerboukha, and M. Skorobogatiy, "3D printed hollow core terahertz Bragg waveguides with defect layers for surface sensing applications," *Opt. Express*, vol. 25, no. 4, pp. 4126–4144, Feb. 2017.
- [10] B. Hong, N. Chudpooti, P. Akkaraekthalin, N. Somjit, J. Cunningham, and I. Robertson, "Investigation of electromagnetic mode transition and filtering of an asymptotically single-mode hollow THz Bragg fibre," *J. Phys. D, Appl. Phys.*, vol. 51, no. 30, p. 305101, 2018.
- [11] B. Hong et al., "Low-loss asymptotically single-mode THz Bragg fiber fabricated by digital light processing rapid prototyping," *IEEE Trans. THz Sci. Technol.*, vol. 8, no. 1, pp. 90–99, Jan. 2018.
- [12] A. Kaur, J. C. Myers, M. I. M. Ghazali, J. Byford, and P. Chahal, "Affordable terahertz components using 3D printing," in *Proc. IEEE 65th Electron. Compon. Technol. Conf. (ECTC)*, San Diego, CA, USA, May 2015, pp. 2071–2076.
- [13] S. Pandey, B. Gupta, and A. Nahata, "Terahertz plasmonic waveguides created via 3D printing," *Opt. Express*, vol. 21, no. 21, pp. 24422–24430, 2013.
- [14] A. I. Hernandez-Serrano and E. Castro-Camus, "Quasi-Wollaston-prism for terahertz frequencies fabricated by 3D printing," *J. Infr., Millim., Terahertz Waves*, vol. 38, pp. 567–573, May 2017.
- [15] Z. Wu, J. Kinast, M. E. Gehm, and H. Xin, "Rapid and inexpensive fabrication of terahertz electromagnetic bandgap structures," *Opt. Express*, vol. 16, no. 21, pp. 16442–16451, Oct. 2008.
- [16] S. F. Busch, M. Weidenbach, M. Fey, F. Schäfer, T. Probst, and M. Koch, "Optical properties of 3D printable plastics in the THz regime and their application for 3D printed THz optics," *J. Infr., Millim., Terahertz Waves*, vol. 35, pp. 993–997, Dec. 2014.
- [17] M. S. Alsoufi and A. E. Elsayed, "How surface roughness performance of printed parts manufactured by desktop FDM 3D printer with PLA+ is influenced by measuring direction," *Amer. J. Mech. Eng.*, vol. 5, no. 5, pp. 211–222, 2017.
- [18] A. Sachdeva, S. Singh, and V. S. Sharma, "Investigating surface roughness of parts produced by SLS process," *Int. J. Adv. Manuf. Technol.*, vol. 64, pp. 1505–1516, Feb. 2013.
- [19] M. Schmid, A. Amado, and K. Wegener, "Polymer powders for selective laser sintering (SLS)," *AIP Conf. Proc.*, vol. 1664, p. 160009, May 2015.
- [20] B. C. Gross, J. L. Erkal, S. Y. Lockwood, C. Chen, and D. M. Spence, "Evaluation of 3D printing and its potential impact on biotechnology and the chemical sciences," *Anal. Chem.*, vol. 86, no. 7, pp. 3240–3253, Jan. 2014.
- [21] R. Udrioiu and L. A. Mihail, "Experimental determination of surface roughness of parts obtained by rapid prototyping," in *Proc. 8th WSEAS Int. Conf. Circuits, Syst., Electron., Control Signal Process.*, Puerto De La Cruz, Spain, 2009, pp. 283–286.
- [22] J. D. Kechagias and S. Maropoulos, "An investigation of sloped surface roughness of direct Poly-Jet 3D printing," in *Proc. Int. Conf. Recent Adv. Mech., Mechatronics Civil, Chem. Ind. Eng. J.*, 2015, pp. 150–153.
- [23] A. Kampker, K. Kreisköther, and C. Reinders, "Material and parameter analysis of the PolyJet process for mold making using design of experiments," *Int. J. Chem., Mol., Nucl., Mater. Metall. Eng.*, vol. 11, no. 3, pp. 242–249, 2017.
- [24] D. R. Bacon et al., "Free-space terahertz radiation from a LT-GaAs-on-quartz large-area photoconductive emitter," *Opt. Express*, vol. 24, no. 23, pp. 26986–26997, 2016.
- [25] Y. C. Shen, P. C. Upadhyaya, E. H. Linfield, and H. E. Beere, "Ultrabroadband terahertz radiation from low-temperature-grown GaAs photoconductive emitters," *Appl. Phys. Lett.*, vol. 83, no. 15, p. 3117, Oct. 2003.
- [26] Y. C. Shen et al., "Generation and detection of ultrabroadband terahertz radiation using photoconductive emitters and receivers," *Appl. Phys. Lett.*, vol. 85, no. 2, p. 164, Jul. 2004.
- [27] High-Power, Coherent Company. (Apr. 2016). *Industrial and Fiber Laser Solutions Provider for Materials Processing and Scientific Markets*. [Online]. Available: https://edge.coherent.com/assets/pdf/COHR_Vitara_DS_0416revC_3.pdf
- [28] Y.-S. Jin, G.-J. Kim, and S.-G. Jeon, "Terahertz dielectric properties of polymers," *J. Korean Phys. Soc.*, vol. 49, no. 2, pp. 513–517, 2006.
- [29] M. N. Afsar, "Dielectric measurements of millimeter-wave materials," *IEEE Trans. Microw. Theory Techn.*, vol. MTT-32, no. 12, pp. 1598–1609, Dec. 1984.
- [30] S. P. Mickan and X.-C. Zhang, "T-ray sensing and imaging," *Int. J. High Speed Electron. Syst.*, vol. 13, no. 2, pp. 601–676, Jun. 2003.
- [31] I. Pupeza, R. Wilk, and M. Koch, "Highly accurate optical material parameter determination with THz time-domain spectroscopy," *Opt. Express*, vol. 15, no. 7, pp. 4335–4350, Mar. 2007.
- [32] Formlabs Company. (Apr. 2018). *High Resolution SLA and SLS 3D Printers for Professionals*. [Online]. Available: <https://formlabs.com>
- [33] Stratasys Company. *3D Printing & Additive Manufacturing*. [Online]. Available: <https://www.stratasys.com>
- [34] Desktop, EnvisionTEC Company. *Professional and Industrial 3D Printers*. [Online]. Available: <https://www.envisiontec.com>
- [35] A. Argyros, "Microstructures in polymer fibres for optical fibres, THz waveguides, and fibre-based metamaterials," *ISRN Opt.*, vol. 2013, Oct. 2012, Art. no. 785162.



NATTAPONG DUANGRIT was born in Chiangmai, Thailand, in 1991. He received the B.Eng. degree from the Rajamangala University of Technology Thanyaburi, in 2014, where he is currently pursuing the Ph.D. degree, supported by the Thailand Research Fund through the Royal Golden Jubilee Ph.D. Program. His main research focuses on the application of 3D printing technology for a millimeter-wave and THz devices, and substrate integrated waveguide applications.



BINBIN HONG (S'16) was born in Zhejiang, China, in 1990. He received the B.Sc. degree in physics, and the M.Sc. degree in plasma physics from Sichuan University, Chengdu, China, in 2011 and 2014, respectively, and the Ph.D. degree from the University of Leeds, Leeds, U.K. His research interests include millimetre-wave and terahertz circuits and device, lab-on-a-chip terahertz microfluidic sensing, and terahertz super-resolution near-field microscopy.



ANDREW D. BURNETT received the Ph.D. degree in electronic and electrical engineering from the University of Leeds, in 2008, after completing his studies in chemistry with forensic science at the University of Bradford, in 2004. Then, he continued his work at the University of Leeds, first, as a Postdoctoral Fellow, funded firstly under the FP6 TERANOVA Project, and then under a Leverhulme Trust Project, to understand the THz spectral properties of protein crystals. In 2015,

he moved to the School of Chemistry as a Teaching Fellow for Physical Chemistry. In 2017, he became a University Academic Fellow. In 2011, he was a recipient of an EPSRC Postdoctoral Fellowship. He moved to the Faculty of Biological Sciences, University of Leeds, where he continued his work on the THz spectra of biological molecules. In 2016, he received an EPSRC Early Career Fellowship.



PRAYOOT AKKARAEKTHALIN (M'98) received the B.Eng. and M.Eng. degrees in electrical engineering from the King Mongkut's University of Technology North Bangkok (KMUTNB), Bangkok, Thailand, in 1986 and 1990, respectively, and the Ph.D. degree from the University of Delaware, Newark, DE, USA, in 1998. From 1986 to 1988, he was a Research and Development Engineer with Microtek Co., Ltd., Thailand. In 1988, he joined the Department of

Electrical Engineering, KMUTNB. His current research interests include RF/microwave circuits, wideband and multiband antennas, telecommunications, and sensor systems. He has authored or co-authored over 40 international journals, more than 200 conference papers, and four books/book chapters. He was the Editor-in-Chief for the ECTI Transactions, from 2011 to 2013. He is a member of the IEICE Japan, ECTI, and EEAAT Associations Thailand. He was the Chairman of the IEEE MTT/AP/ED Thailand Joint Chapter, from 2007 to 2010, and the Vice President and President of the ECTI Association, Thailand, from 2012 to 2013 and from 2014 to 2015, respectively. He is currently the Head of the Senior Research Scholar Project, under the Grant from the Thailand Research Fund (2015–2017).



IAN D. ROBERTSON (F'12) received the B.Sc. (Eng.) and Ph.D. degrees from King's College London, London, U.K., in 1984 and 1990, respectively.

From 1984 to 1986, he was with the GaAs MMIC Research Group, Plessey Research, Caswell, U.K. After that, he returned to King's College, initially as a Research Assistant, working on the T-SAT Project, subsequently as a Lecturer, leading the MMIC Research Team, and becoming a Reader, in 1994. In 1998, he became a Professor of microwave subsystems engineering with the University of Surrey, where he established the Microwave Systems Research Group, and was a Founding Member of the Advanced Technology Institute. In 2004, he was appointed to the Centenary Chair in Microwave and Millimetre-Wave Circuits of the University of Leeds. He was the Director of Learning and Teaching, from 2006 to 2011, and also the Head of the School, from 2011 to 2016.

Dr. Robertson was the General Technical Programme Committee Chair for the European Microwave Week, in 2011 and 2016, respectively.



NUTAPONG SOMJIT (M'10) received the Dipl.Ing. (M.Sc.) degree from the Dresden University of Technology, in 2005, and the Ph.D. degree from the KTH Royal Institute of Technology, in 2012. Then, he returned to Dresden University of Technology to lead a research team in micro-sensors and MEMS ICs for the Chair for Circuit Design and Network Theory. In 2013, he was appointed as a Lecturer (Assistant Professor) with the School of Electronic and Electrical

Engineering, University of Leeds. His main research focuses on integrated smart high-frequency components, heterogeneous integration, and low-cost microfabrication processes. He was a recipient of the Best Paper Award (EuMIC Prize) at the European Microwave Week, in 2009. He was awarded a Graduate Fellowship from the IEEE Microwave Theory and Techniques Society (MTT-S), in 2010 and 2011, respectively, and the IEEE Doctoral Research Award from the IEEE Antennas and Propagation Society, in 2012. Since 2013, he has been a member of the International Editorial Board of the International Journal of Applied Science and Technology. He was appointed as a member of the Engineering, Physical and Space Science Research Panel of the British Council, in 2014. In 2016, he was the Chair of the Student Design Competition for the European Microwave Week. In 2018, he was appointed as an Associate Editor of *Electronics Letters*.

...